NATIONAL RADIO ASTRONOMY OBSERVATORY
Green Bank, West Virginia

INTERNAL REPORT

AN EXPERIMENTAL CHECK OF ANTENNA TOLERANCE THEORY USING RADIO ASTRONOMICAL TECHNIQUES

P. G. MEZGER

APRIL 4, 1965

DRAFT: 4/5/65:pj

An Experimental Check of Antenna Tolerance Theory Using Radio Astronomical Techniques

P.G. Mezger

National Radio Astronomy Observatory*
Green Bank, West Virginia

Abstract

The antenna tolerance theory describes the effect of systematic and random mechanical deviations of an antenna on its radio frequency performance. The reflector surfaces of the NRAO 85(I)-foot and 300-foot antennas have been measured at different elevation angles. The radio frequency characteristics of these antennas at various wavelengths have been measured using radio astronomical techniques, which is reviewed in Section II. Combining electrical and mechanical measurements allows an experimental check of antenna tolerance theory. The effect of systematic deviations is discussed in Section III and the effect of random deviations is discussed in Section IV. In all cases good agreement between theory and experimental result has been obtained.

I. Introduction

The antenna tolerance theory describes the effect of systematic and random mechanical deviations of an antenna on its radio frequency performance. The results of this theory are of great interest for both radio astronomical observations at high frequencies and with large radio telescopes, and for the development of future large radio telescopes.

---

*The National Radio Astronomy Observatory is operated by Associated Universities, Inc., under contract with the National Science Foundation.

In order to check the predictions of antenna tolerance theory, one has to know first the mechanical characteristics of an antenna. The reflectors of the NRAO 85(I)-foot and 300-foot telescopes have been measured using a photogrammetric method*. Target points were marked on the reflector surface, whose positions in an x,y,z coordinate system were measured at different zenith distances of the reflector axis. Applying the method of "least squares" the "best fit" paraboloid and the deviation d_i of each target point i from this best fit paraboloid were computed. Figure 1a shows a histogram of the measured deviations for both telescopes at different zenith distances. The curves in the histogram represent the corresponding gauss distribution, computed for the RMS deviation

$$\sqrt{\overline{d^2}} = \frac{1}{\sqrt{N}} \left[\sum_{i=1}^{N} \overline{d_i^2} \right]^{1/2} \tag{1}$$

with N the total number of measured target points. The target points lay on concentric circles. By computing the RMS reflector deviations in the different ring-shaped zones we obtain the RMS reflector deviation as a function of the normalized distance from the axis of symmetry of the paraboloid. (Fig. 1b)

If the reflector position is changed, the random reflector deviations are superimposed by large scale deflections which cause both changes of the focal length and the direction of the electrical axis. The photogrammetric calibration shows that the focal length of the 85(I)-foot telescope changes

---

* The photogrammetric reflector calibration has been done by D. Brown Associates, Inc., Eau Gallie, Florida.

by about 4 cm between zenith and horizon; the focal length of the 300-foot telescope changes by even 11 cm. Combined mechanical and radio frequency measurements have shown [1] that the beam tilt of the 300-foot telescope with increasing zenith distance is considerably larger than would be expected from the measured sag of the feed support legs. This can be only understood by a large scale deflection of the reflector which amplifies the effect of the lateral defocusing of the feed. The effect of lateral and radial defocusing of the phase center on the radio frequency performance of a paraboloidal reflector antenna are discussed in Section III.

The basic relations of antenna tolerance theory, which connect random reflector deviations with the radio frequency characteristics of the radio telescope, have been derived by Ruze [2]. Skolnik [3] and Jasik [4] give in their books good reviews of most of the publications concerning antenna tolerance theory. We will use in Section III only Ruze's results, although in a slightly modified form. Only for the computation of the error pattern we will use an approximation, introduced by Scheffler [5] in his tolerance theory for optical telescopes, since it yields more convenient results.

The measurement of the radio frequency characteristics of large radio telescopes is best done by radio astronomical techniques. Part of this technique is presented in earlier publications [6],[7]. Kuzmin and Salomonovich [8] have recently published a book "Radio Astronomical Method of the Measurement of Antenna Parameters" which, however, has not yet been translated. We will briefly outline in Section II the methods used in our investigation. The concept of antenna stray factor, beam efficiency and convolution integral-quantities which are widely used in radio

astronomical observing techniques will be briefly discussed in the appendix of this paper. We also refer to the papers of Bracewell [9] and Ko [10].

II. Antenna Measurements Using Radio Astronomical Techniques

The basic quantity in determining gain and effective area of an antenna is the integral over its power far field pattern. As shown in Appendix I, this integral can be split up in two parts and the antenna solid angle can be expressed by the main beam solid angle Ω_m and the main beam stray factor β_m

$$\Omega = \int_{4\pi} f d\Omega = \Omega_m/(1-\beta_m) \tag{2}$$

If the main beam can be approximated by a two-dimensional gaussian function with HPBW (half power beam width) Θ_E and Θ_H in the main planes, then $\Omega_m = 1.133\ \Theta_E\Theta_H$. The stray factor has a simple physical interpretation. If the (lossless) antenna is placed inside a black body enclosure with wall temperature T, then the antenna temperature is equal to the wall temperature $T_A = T$. The part $(1-\beta_m)T$ of the antenna temperature is due to the radiation received within in the main beam, the part $\beta_m T$ is due to the radiation received within the stray region of the antenna pattern.

Often a more detailed information is wanted as to the contribution of different parts of the antenna stray region to the main beam stray factor. Then a stray factor for the special region i can be defined by the integral

$$\beta_i = \frac{1}{\Omega} \int_{\text{region } i} f\ d\Omega \tag{3a}$$

If $\sum_i$ region i = total stray region, then

(3b) $$\sum_i \beta_i = \beta_I + \beta_{II} + \ldots = \beta_m$$

The radiation efficiency η_R takes into account the losses in the feed and in the reflector of the antenna. The definition of antenna gain includes already these losses, $G = \eta_R D$ with $D = 4\pi/\Omega$ the directivity of the antenna. In most practical cases one has to deal therefore with the product of radiation efficiency times main beam stray factor, and it has been found convenient to define a new quantity

(4) $$\eta_\beta = (1-\beta_m)\eta_R$$

as beam efficiency. It is shown in Appendix I how antenna gain, effective area and other related quantities can be expressed in terms of main beam solid angle and beam efficiency. In the following it will be outlined shortly how these antenna characteristics can be measured using radio astronomical techniques.

1. Antenna Gain and Related Characteristics

Considerable effort has been spent in radio astronomy in order to make absolute flux density measurements of the strongest radio sources or absolute measurements of the black body temperature of the sun, the moon and the planets. We refer to [11] for an analysis of flux densities of radio sources in the meter and longer dcm wavelength range. The spectra of the strongest nonthermal radio sources in the cm wavelength range have been

analyzed in [12]. For a review of the black body temperatures of the planets and their variation with time and frequency, see e.g. [13]; for a review of the black body temperatures of the sun and the moon, see [8],(Tables I and II).

The flux density of radio sources is given in W/m^2Hz or in flux units with 1.f.u. = 10^{-26} W/m^2Hz. The antenna temperature which a radio source produces in a radio telescope is measured relative to the background antenna temperature, which is due to both the extra-terrestrial and ground radiation and to the ohmic losses. For a review of radiometers used for the measurement of antenna temperatures and of the methods used for their calibration, see e.g. [14].

The relation between flux density S_ν and maximum antenna temperature T_A, produced by this source in a radio telescope with effective area A, is given by

$$S_\nu = \frac{2kT_A}{A} \frac{\Omega_s}{\Omega_s'} \tag{5}$$

where k = 1.38 10^{-23} $Ws/^\circ K$ the Boltzmann constant. The source size correction factor Ω_s/Ω_s' is discussed in Appendix II. If the HPW of the radio source is small as compared to the HPBW of the antenna, $\Omega_s' \approx \Omega_s$ and the source size correction factor becomes unity; in all other cases $\Omega_s' < \Omega_s$ and the source size correction factor is larger than unity. This factor is computed for two different source models in Appendix II and can be used in conjunction with the source models given in [12], as long as $\Omega_s/\Omega_s' < 1.3$. If the correction factor assumes larger values it is advisable to apply a numerical integration of the mapped antenna temperature distribution [12] which yields the result

$$S_\nu = \frac{2K}{\lambda^2 \eta_B} \int_{\text{main beam region}} T_A \, d\Omega$$

If the main beam solid angle is known the effective antenna area can be converted into beam efficiency and vice versa using eq. (I,6).

Flux densities and brightness temperatures of radio sources are always referred to outside the atmosphere, and in the case of linear polarization of the source, to the total flux density. If S_o is the flux density outside the atmosphere the flux density S observed at the surface of the earth at a zenity distance z is

$$S = S_o p^{F(z)} \tag{7}$$

p is the transmission coefficient at the zenith, F(z) is the air mass function [15] which can for $z \leq 70°$ be approximated by 1/cos z. For numerical values of the zenith transmission coefficient, see Appendix III.

Let $\bar{S}$ be the total flux density of a radio source which has the degree of polarization p and the polarization angle φ_p. The position angle φ_E of the electric plane of a linearily polarized antenna is counted counter-clockwise, starting at north. The flux density observed with this position angle of the electric plane is then

$$S(\varphi_E) = \bar{S} \left[1 + p - 2p \sin^2 (\varphi_p - \varphi_E)\right] \tag{8}$$

The polarization parameters p and φ_p of many radio sources are compiled by Howard et als [11].

In the short cm-and in the mm-wavelength range the thermal radiation of planets seems to yield the most convenient calibration source. The blackbody temperature T_{bb} of a radio source is connected with the antenna temperature observed with a radio telescope with beam efficiency η_B and effective area A by

$$T_A = \eta_B T_{bb} \frac{\Omega_s'}{\Omega_m} = T_{bb} \Omega_s' \frac{A}{\lambda^2} \tag{9a}$$

As a first approximation the brightness distribution of a planet may be considered as a disk distribution and hence eq. (II,7b) can be used to compute Ω_s', using for R the optical radius of the planet. In the case of the moon and the sun, their diameters will be often considerably larger than the diameter of the main beam region. Assuming that radiation is only received by the main beam, one obtains $\Omega_s' = \Omega_m$, and hence

$$T_A = \eta_B T_{bb} \qquad \text{for } 2R = \text{diameter of main beam area} \tag{9b}$$

If the level of the first side lobes is below -23 dB, this relation holds approximately also for the case that the source solid angle is considerably larger than the main beam area. For lower side lobe levels, however, the radiation received in the side lobes will contribute considerably to the antenna temperature and the beam efficiency obtained from eq. (9b) will be larger than when measured with a point source using eq. (9a) or (5). This difference can be used (see Section IV) to compute the level of the nearby side lobes, and hence the contribution of the error pattern.

2. Antenna HPBW and Main Beam Solid Angle

With the gaussian approximation of the main beam, eq. (I,2), the main beam solid angle can be directly computed from the HPBW's of the two principal planes of the antenna $\Omega_m = 1.133\ \Theta_E \Theta_H$ (eq. I,3). If the gauss approximation holds down to a level of -17 dB the error introduced by integrating the main beam from $-\infty$ to $+\infty$ rather than within the main beam region is less than 2%. If there is, however, a considerable departure of the measured power pattern from the gaussian approximation already at levels of -10 dB and less, the measured main beam pattern should be numerically integrated.*

Since the drift velocity of radio sources is always very well known, it is easy to perform precise measurements of angular distances by means of drift curves. As long as the HPW of the radio source is less than one tenth of the antenna HPBW the effect of beam broadening can be neglected and the HPW of the drift curve, after being converted in angular distances, yields directly the antenna HPBW. If this assumption is no longer valid, eq. (II,4) can be used to correct for the beam broadening, provided the true source distribution can be approximated by either a gauss or disk model. At very high frequencies where no strong point sources are available, drift curves with the sun or the moon can be used to determine approximately the main beam pattern and antenna HPBW (see Appendix II).

3. Stray Factors

If the measurements, described in the preceding sections, have been performed, it is easy to compute the main beam stray factor using any of

---

* For computations of this type it is convenient to remember that 4π steradian = 41 253 [degrees of arc]^2.

the relations given in Appendix I, provided the radiation efficiency η_R is known. It is in practice extremely difficult to measure this quantity. Computations made for decimeter wavelengths have shown that for parabolic and horn antennas η_R deviates less than 0.5% from unity. In the longer cm-wavelength range the radiation efficiency is generally estimated to be about 0.99. At still shorter wavelengths, however, η_R may deviate considerably from unity due to the increasing losses in both feed and reflector. With the antenna pointed at zenith the measured absolute antenna temperature can be related to the radiation temperature of the ground and the atmosphere by means of eq. (II,2). One obtains

$$(10) \qquad T_A(z = 0°) = \eta_B T_z + (1-\eta_R)\ T_L + \eta_R \sum_i \beta_i \bar{T}_i$$

T_z is the radiation temperature of the zenith region given by eq. (III,2). T_L is the temperature of the ohmic losses in feed and reflector. $\bar{T}_i$ is the average brightness temperature in the stray region i.

Using a simplified, but for many cases satisfactory, model of the antenna pattern, we divide the total stray region into a Region I, which comprises the nearby side lobes approximately down to the level of a corresponding isotropic antenna, and a Stray Region II, which comprises the rest of the total stray region, and where we may assume a constant level of the side lobes. In some cases it may be desirable to include a Stray Region III in this model which comprises the spill over side lobes. The border line between Stray Region I and II depends on the taper of the feed pattern, but for pencil-beam antennas with HPBW's $< 1°$ and with an edge

taper of about -16 dB it has been found that this border line lies at an angular distance between 30 and 60 times the HPBW of the main beam. With the antenna pointed at zenith the brightness temperature in Stray Region I can therefore be assumed to be identical with the brightness temperature T_z at zenith.

As long as the area of Stray Region I is small as compared to 2π, one-half of the Stray Region II looks into the sky, whose average brightness temperature $\overline{T}(z)$ is given by eq. (III,3b); the other half looks into the ground, whose average brightness temperature $\overline{T}_g$ has to be estimated. (See Appendix III.) Eq. (10) can then be written in the form

$$(11) \quad T_A(z = 0°) = \eta_R(1-\beta_m)\, T_z + \eta_R \left\{ \beta_I T_z + \beta_{II} \frac{\overline{T}(z) + T_g}{2} \right\} + (1-\eta_R)\, T_L$$

The absolute antenna temperature is measured by substituting cooled loads in the place of the antenna feed. With the relation $\beta_I + \beta_{II} = \beta_m$ eq. (11) can be used to compute β_I and β_{II} if β_m is known. The accuracy of this determination of the stray factors depends on the accuracy with which both the average brightness temperatures in the stray regions and the radiation efficiency can be estimated. It has been found in this way that for horn feeds with edge tapers of about -16 dB used in the NRAO telescopes at wavelengths where the reflectors can still be considered to be perfect, the main beam stray factors have values between 0.20 and 0.30, with the stray factors β_I and β_{II} contributing about 50% each. With special low-noise

feeds or in the case of Cassegrain antennas both the relative contribution and the absolute value of β_{II} can be considerably reduced. On the other hand phase errors caused by systematic or random mechanical deviations (see Sections III and IV) increase mainly the nearby side lobe level, which results in an increase of the absolute values of the main beam stray factor and the stray factor β_I whereas β_{II} remains virtually unaffected.

By measuring and evaluating the absolute antenna temperature at various zenith distances and estimating the average brightness temperatures in the different stray regions, it is possible to obtain rather detailed information on the average side lobe levels of different regions of the antenna pattern.

The antenna temperature measured at the zenith (eq. 11) is very sensitive to a change in the radiation efficiency and by inserting for the stray factors values of comparable antennas this relation may be used to estimate the radiation efficiency of radio telescopes at very high frequencies.

III. Systematic Errors

We are mainly concerned with that systematic error introduced by a deviation of the phase center of the feed from the focal point of the paraboloidal reflector (defocusing). Numerical computations of the pattern of defocused paraboloidal antennas by Baars* have shown that for small deviations the total defocusing can be decomposed in a radial and

---

* Private communication

axial component, Δf_{rad} and Δf_{ax}, and then the effect of the defocusing on the gain (but not on the pattern) can be treated separately so that $G(\Delta f) = G(\Delta f_{ax})\ G(\Delta f_{rad})$. A pure radial defocusing introduces a linear and cubic phase error in the aperture plane. The linear phase term causes a tilt of the beam in the direction opposite to the deviation of the phase center of the feed. The angle of this beam tilt is given by $\Theta = B \cdot \text{arc tg}\ (\Delta f_{rad}/f)$ with Δf_{rad} the distance between phase center and focal point of the paraboloid, f the focal length and $B \leq 1$ the beam factor. The cubic phase error causes a decrease in gain and an increase in both the HPBW of the main beam and in the level of side lobes, especially the "coma lobe." The off-axis characteristics of parabolic antennas have been investigated experimentally by Kelleher and Coleman [16] and numerically by Ruze [17]. For small radial defocusing (about four times the HPBW) we found a good agreement with Ruze's computations. Figure 2 shows the main beam pattern of three identical feeds for 1410 MHz mounted in the focal plane of the 300-foot telescope. The phase center of the central feed coincides with the focal point of the reflector, whereas, the two outer feeds are radially defocused corresponding to angular distances of about 3.5 (for the east feed) and 4 (for the west feed) times the HPBW of the central feed [18]. Since the 300-foot reflector is no longer perfect at this frequency, the coma lobes are superimposed on the error pattern and their levels are therefore higher than predicted from Ruze's computation.

A pure axial defocusing results in a square phase error in the aperture plane, with $\beta = \frac{2\pi}{\lambda} \Delta f_{ax}(1-\cos \Theta_0)$ the phase difference between central and edge ray. λ is the wavelength, Δf_{ax} the distance between phase center of the feed and focal point of the reflector and Θ_0 the aperture

angle. One computes for the decrease in gain

$$(12a) \qquad G/G_0 = \left[\frac{\sin \beta/2}{\beta/2}\right]^2 \approx 1-\beta^2/12 + \ldots \text{ for uniform illumination}$$

and

$$(12b) \qquad G/G_0 = \left[\frac{\sin \beta/2}{\beta/2}\right]^4 + 4/\beta^2 \,[\sin \beta/\beta - 1]^2 \approx 1-\beta^2/18 + \ldots$$

for a $(1-r^2)$ tapered illumination.

By measuring the relative change of the antenna temperature of a point source while moving the phase center of the feed along the axis of symmetry of the reflector, these relations can easily be checked. This is indeed the standard procedure to focus radio telescopes.

Figure 3 shows focusing curves measured with the 85-foot telescope and point sources at λ = 2cm and 6 cm, respectively. Curve (a) has been computed from eq. (12b), and the points have been measured with point sources at 2 and 6 cm wavelength. At very high frequencies it becomes difficult to find strong point sources for focusing; the only strong radio sources at these frequencies -- sun and moon -- having diameters of about 30 minutes of arc. If such extended souces are used for the focusing of a radio telescope one has to consider not only the decrease in gain but also the increase in the HPBW and in the side lobe level. The relation between the brightness temperature of an extended radio source and the corresponding antenna temperature in a radio telescope is given by eq. (II,6a) and can be rewritten in the form

$$T_A = \eta_\beta \frac{\Omega'_s}{\Omega_m} T_M = \frac{\eta_R}{4\pi} \Omega'_s G \tag{13}$$

If the diameter of the extended source is approximately equal to the main beam region of the antenna, then $\Omega'_s \approx \Omega_m$, and one can see that the decrease in gain as given by eq. (12) is partly compensated by the increase in HPBW. This can be seen from curve (b) in Fig. 3, which has been measured with the 85-foot telescope at 5 GHz (Θ_A = 10') and with the moon. If the diameter of the extended source is considerably larger than the main beam region of the antenna the compensation of decrease in antenna gain becomes even stronger since the radiation received by the nearby side lobes contribute also to the antenna temperature. This effect is shown clearly by curve (c) in Fig. 3, which has been measured with the 85-foot telescope at 14.5 GHz (Θ_A = 3.35') and with the moon. It is found, however, that the symmetry line of both focusing curves measured with the moon do not coincide with the symmetry line of the focusing curves measured with point sources, what may introduce a considerable error in the focusing of a radio telescope with an extended source. The criterium of smallest HPBW which can be tested with drift curves through the sun or the moon [19] may then be a better way for the fine adjustment of the focus position.

IV. Random Errors

Under conditions which will be discussed later, the effect of random phase errors in the aperture plane of a radio telescope on its radio frequency characteristics can be fully described if the square phase error

$\overline{\delta^2}$ and the correlation length ℓ of the phase errors are known. Ruze [2] defines the correlation length as the average distance in the aperture plane at which the phase errors become statistically independent. In Scheffler's theory [5] the correlation length means the shortest spatial wavelength at which the Fourier spectrum of the random phase errors has values virtually different from zero.

Ruze and Scheffler have shown that the power pattern of an aperture with random phase errors can be represented by the superposition of the diffraction pattern f_D with an error pattern f_E whose shape depends on both $\overline{\delta^2}$ and ℓ

$$\overline{f(\Theta,\varphi)} = f_D(\Theta,\varphi) + f_E(\Theta,\overline{\delta^2},\ell) \tag{14}$$

The error pattern is given by the expression

$$f_E(\Theta,\overline{\delta^2},\ell) = \frac{4\ell^2}{\eta_A D^2} \sum_{n=1}^{\infty} \frac{[\delta^2]^{n-1}}{n!\,n} \exp\left\{-\pi^2\ell^2\Theta^2/n\lambda\right\} \tag{15}$$

$$\approx \frac{4\ell^2}{\eta_A D^2}\left[e^{\overline{\delta^2}} - 1\right] \cdot \begin{cases} \exp\left\{-\pi^2\ell^2\Theta^2/\lambda^2\right\} & \overline{\delta^2} \leq 1 \\ \dfrac{1}{\delta^2} \exp\left\{-\pi^2\ell^2\Theta^2/\lambda^2\,\overline{\delta^2}\right\} & \overline{\delta^2} \geq 1 \end{cases}$$

The rigorous expression has been derived by Ruze; the approximation is due to Scheffler. We call the aperture with phase errors imperfect, without phase errors perfect. The antenna solid angle of the imperfect aperture is obtained by integrating eq. (14). With $\Omega_o = \int_{4\pi} f_D \, d\Omega$ the solid angle of the perfect aperture the integration yields,

$$(16) \qquad \Omega = \int_{4\pi} \overline{f(\Theta,\varphi)}\, d\Omega = \Omega_o + \Omega_o(e^{\overline{\delta^2}} - 1) = \Omega_o e^{\overline{\delta^2}}$$

That means that the antenna solid angle of the imperfect aperture has increased by $e^{\overline{\delta^2}}$ as compared to the solid angle of the perfect aperture. The gain of the imperfect (but lossless) aperture is consequently

$$(17) \qquad G = 4\pi/\Omega = G_o e^{-\overline{\delta^2}}$$

with $G_o = 4\pi/\Omega_o$ the gain of the perfect aperture. This is the expression for the decrease in gain due to random phase errors with the mean square value $\overline{\delta^2}$ derived first by Ruze. Note that the decrease in gain does only depend on $\overline{\delta^2}$, not on the correlation length ℓ. It is predicted from theoretical considerations [20] and confirmed by our measurements that even in such extreme cases where the antenna gain has been reduced by a factor of five and more the shape of the main beam is determined by the diffraction pattern of the perfect reflector and is not affected by the random errors. The main beam solid angle of the imperfect aperture is consequently the same as that of the perfect aperture, and the main beam stray factor of the imperfect aperture is

$$(18) \qquad \beta_m = 1 - \Omega_m/\Omega = 1 - \frac{\Omega_m}{\Omega_o}\, e^{-\overline{\delta^2}}$$

with Ω_m and Ω_o the solid angles of the perfect aperture. This relation has also been confirmed by our measurements.

In order to apply the results of this theory to practical antennas one uses the relation between phase error δ and corresponding deviation $\underline{d}$ of the reflector from the "best fit" paraboloid

$$\delta = \frac{2\pi}{\lambda} \; 2d \tag{19}$$

which is approximately valid for shallow reflectors. The target points for the photogrammetric survey of the NRAO reflectors (see Section I) were marked on concentric rings around the vertex of the paraboloid. The RMS deflections of the ring-shaped zones have been computed and are plotted as a function of the normalized distance in the aperture plane in Fig. 1b. Apart from the fact that the target points in the different ring-shaped zones do not represent the same surface elements, it has also to be considered that deviations at distances farther away from the vertex contribute less to the RMS phase error due to the tapering of the feed pattern. Considering these facts one has to weigh the RMS deflection of the k-th ring-shaped zone in the aperture conforming to

$$\overline{d^2} = \frac{\sum_k \overline{d_k^2} \; S_k f_k}{\sum_k S_k f_k} \tag{20}$$

with S_k the area of the k-th ring-shaped zone and f_k the average value of the feed power pattern in this zone. Table 1 shows the weighted and unweighted RMS deviations of the 85(I)- and 300-foot reflectors as computed from the photogrammetric survey

Table 1

Telescope:	85(I)-foot		300-foot		
Zenith distance	0°	90°	0°	30°	51.4°
RMS deviation computed from eq.(1) in mm	3.16	5.71	10.72	12.70	9.47
RMS deviation weighted conf. to eq.(20) in mm	2.75	4.17	12.44	12.63	10.87

The weighting process can increase or decrease the RMS deviation depending on the distribution of the RMS deviations as a function of radial distance. Assuming a tapered illumination of the form $(1-r^2)^p$ it can be easily shown that the weight function reaches its maximum at the distance $r_{max} = (2p + 1)^{-1/2}$. Since a similar reasoning applies to the change of focal length due to surface deviations, this result means that the reflector surface should have its optimum stiffness in the zone around r_{max}.

In order to compare the predictions of antenna tolerance theory with measurements, it is more convenient to consider the aperture efficiency rather than the antenna gain since the aperture efficiency of a perfect reflector is a constant value, provided the feed patterns are identical at any frequency. It should be mentioned, however, that since the gain of a perfect aperture increases with the square of the frequency, the gain of an imperfect aperture as given in eq. (17) attains a maximum value for the wavelength $\lambda_{opt} = 4\pi\sqrt{\overline{d^2}}$. This means that if point sources with frequency independent brightness temperatures--such as some planets--are observed, they will produce their maximum antenna temperature at this wavelength.

Changing from gain to aperture efficiency and substituting eq.(19) one obtains

$$(20) \qquad \eta_A(\lambda) = \eta_{A_o} \exp\{-\bar{\delta}^2\} = \eta_{A_o} \exp\left\{-16\pi^2 \frac{\overline{d^2}}{\lambda^2}\right\}$$

with η_{A_o} the efficiency of the perfect aperture. In order that this equation can be applied to describe the change of the aperture efficiency of an imperfect reflector, the following conditions have to be fulfilled [21]:

1. The deviations from the best fit paraboloid are random and distributed in a Gaussian manner.

2. The errors are uniformly distributed over the antenna aperture.

3. The regions over which the errors are substantially constant (i.e., their correlation length) is large compared to a wavelength.

4. The number of such uncorrelated error regions in the aperture is large (at least 5-10).

An inspection of Figures 1a and b shows that conditions 1 and 2 are fulfilled in the case of the NRAO 85(I)- and 300-foot reflectors, with the exception of the 85-foot reflector at zenith distance z = 90°, where the RMS deviation of the ring-shaped zones at the edge of the aperture is about three times that of the vertex zone. The contour map representation (Fig. 4) of the reflector deviations at zenith and at horizon position (z = 0° and 90°, respectively) reveals that this departure from a uniform

error distribution is caused by a large scale deflection which causes the northern and southern quadrant of the reflector to be bent outward and the eastern and western quadrant to be bent inward, resulting in an astigmatism of the total reflector. From an inspection of the contour map at z = 90° on the other hand one feels, at least qualitatively, that the conditions 3 and 4 are fulfilled. This statement will be yet proved quantitatively.

The aperture efficiency of both NRAO telescopes has been measured at various frequencies, using radio astronomical techniques described in Section II. In order to obtain the aperture efficiency η_{A_o} of the perfect reflector, log $\eta(\lambda)$ was plotted over $1/\lambda^2$ and a straight line was fitted through the measured points. We found in this way

Table 2

Telescope:	85(I)-ft	300-ft
Aperture efficiency of the perfect reflector $\eta_A(\lambda\to\infty)$	58%	67%

With these values and the weighted RMS deviations taken from Table 1, eq. (20) was evaluated (full curves in Figs. 5a and b). The measured points are plotted in Fig. 5, together with their error bars. At most frequencies feeds with an edge taper between -16 and -18 dB and similar feed patterns were used, with the exception of the 85-foot telescope at 5 GHz, where a scalar feed* with the same edge taper but a more favorable

*Supplied by TRG, Inc.

shape of the feed pattern, and at 14.5 GHz, where a horn feed with an edge taper of only -14 dB were used. In the case of the 300-foot telescope, the predicted change of aperture efficiency agrees well with our measurements. In the case of the 85(I)-foot reflector the measured points follow qualitatively eq. (20), but are best fitted by a curve which corresponds to an effective reflector deviation of 1.75 mm rather than the computed RMS value of 2.75 mm. We have reason to believe that the RMS reflector deviation derived from the measurement of the aperture efficiency as a function of wavelength yields better values than any other type of direct measurement, as has been suggested by Ruze [21].

The reflector surface of most telescopes has been adjusted with the telescope axis pointed at the zenith, and it is therefore expected that the RMS surface deviation increases with increasing zenith distance. This effect can be seen very clearly in the case of the 85-foot telescope, although the increase in the RMS reflector deviation is partly due to large scale deflections, and therefore violates the conditions 3 and 4 for the applicability of eq. (20). In order to measure the increase in the effective RMS reflector deviation, the aperture efficiency of the two 85-foot telescopes presently in operation at the NRAO has been measured as a function of zenith distance z at the frequency 14.5 GHz. After correcting for the attenuation of the atmosphere it was found that the aperture efficiency of the 85(I)-foot telescope at the horizon has decreased to 29% of its value at the zenith; that of the 85(II)-foot telescope has decreased to 77% of its zenith value. The variation of the aperture efficiency with zenith distance is approximately proportional to cos z.

Since both telescopes have at the zenith the same aperture efficiency (about 30%), it can be concluded that their RMS reflector deviation at this position is the same, viz. 1.75 mm, as has been derived from the best fitting curve in Fig. 5a. Assuming that the decrease of the aperture efficiency at the zenith distance z is caused by an increase of the RMS reflector deviations by the amount $\sqrt{\overline{\Delta d^2}}$ -- where ($d^2(z) = \overline{d^2}(0) + \overline{\Delta d^2}$)-- one obtains from eq. (20)

$$(21) \quad \sqrt{\overline{\Delta d^2}} = [\ln(\eta_A(0)/\eta_A(z))]^{1/2} \lambda/4\pi = 0.121 \lambda [\log (\eta_A(0)/\eta_A(z))]^{1/2}$$

and, with the measured decrease of aperture efficiency, an increase of the RMS reflector deviation of $\sqrt{\overline{\Delta d^2}}$ = 1.84 mm (85(I)-foot) and 0.83 mm (85(II)-foot) is computed. The photogrammetric measurement gives an increase of the weighted RMS deviations of 1.42 mm (Table 1) for the 85(I)-foot telescope. This result means that eq. (20) describes the effect of an increase in the RMS reflector deviations correctly, even if condition 4 is not completely fulfilled.

A direct determination of the correlation length of the reflector deviations from the photogrammetric measurements is not possible since -- as will be shown -- the average distance between the target points on the reflector is larger than the correlation length. Figure 6 shows the error pattern of the 300-foot reflector computed from eq. (15) with the parameters given in Fig. 6 and for various values of the correlation length. This figure shows clearly that with increasing correlation length the HPW

of the error pattern gets smaller and its peak value gets higher. The integral of the error pattern does, however, not depend on the correlation length as can be seen from eq. (16).

It has been shown in Section II,1 that the beam efficiency measured with an extended source like the sun or the moon, using eq. (9b), will usually lead to a larger value than if the aperture efficiency is measured with a point source, due to the fact that the antenna receives radiation not only in the main lobe but also in the side lobes. The amount of radiation received by the error pattern can be estimated by integrating eq. (15), and one obtains the relation [1].

$$(22) \qquad \frac{\eta_B' - \eta_B}{\eta_{B_o} - \eta_B} = \begin{cases} 1 - \exp\left\{-\dfrac{\pi^2 \ell^2 R^2}{\lambda^2}\right\} & d \leq \lambda/12.566 \\ 1 - \exp\left\{-\dfrac{\ell^2 R^2}{16\,\overline{d^2}}\right\} & d \geq \lambda/12.566 \end{cases}$$

Here is η_B the beam efficiency of the imperfect reflector, measured with a point source

η_B' the beam efficiency of the imperfect reflector measured with an extended disk source of radious R (in radian)

η_{B_o} the beam efficiency of the perfect reflector

$\overline{d^2}$ the mean square reflector deviation.

If these values are known, the correlation length of the reflector deviations can be determined from eq. (22). We have found in this way the correlation length ℓ = 2.5 meters for the 300-foot telescope, and ℓ = 1.2

meters for the 85(I)-foot telescope. It is interesting to note that in the case of the 300-foot reflector the correlation length corresponds approximately to the average dimension of the individual panels which form the reflector, whereas in the case of the 85-foot reflector the correlation length is considerably shorter than the average panel size.

Assuming now that each target point represents the same area in the aperture plane it can be easily shown that at least $(D/\ell)^2$ target points are needed in order to get a full picture of the reflector deviations. Therefore, at least 500 target points should have been used for the measurement of the 85(I)-foot telescope and 1350 target points for the measurement of the 300-foot reflector, whereas the measurements were made with about 250 and 300 target points, respectively.

A P P E N D I X

I. STRAY FACTOR AND BEAM EFFICIENCY

The power pattern $f(\Theta,\varphi)$ is defined as a function of the spherical coordinates Θ,φ, and is normalized so that $f(0,0) = 1$. The antenna solid angle is defined as the integral of the power pattern over the unity sphere (sphere with r = 1). We separate this integral into two terms

$$(I,1) \qquad \Omega = \int_{4\pi} f \, d\Omega = \int_{\text{main beam}} f \, d\Omega + \int_{\text{stray region}} f \, d\Omega$$

The main beam is defined as the region contained within the first minimum of the power pattern; the stray region is the surface of the unity sphere outside the main beam.

Experience has shown that the main beam of large circular paraboloidal antennas can be approximated with very high accuracy by the function

$$(I,2) \qquad f_m = \exp\left\{-\frac{\xi^2}{\xi_o^2} - \frac{\eta^2}{\eta_o^2}\right\} \quad \text{with} \quad \left.\begin{matrix}\xi_o \\ \eta_o\end{matrix}\right\} = \frac{1}{2\sqrt{\ln 2}} = 0.6006 \left\{\begin{matrix}\Theta_E \\ \Theta_H\end{matrix}\right.$$

Θ_E and Θ_H are the half-power beam widths (HPBW) of the antenna in electric and magnetic plane (in the case of a linearly polarized feed) or the minimum and maximum HPBW (in the case of a circular polarized feed), respectively. Since the angular distances Θ are small, at which the main beam contributes appreciably to the integral, the spherical coordinates Θ,φ have been replaced by the rectangular coordinates ξ,η.

The approximation (I,2) of the main beam allows us to compute the main beam solid angle

$$\text{(I,3)} \qquad \Omega_m = \int_{-\infty}^{+\infty}\int \exp\left\{-\frac{\xi^2}{\xi_0^2}-\frac{\eta^2}{\eta_0^2}\right\} = \frac{\pi}{4\ \ln 2}\,\Theta_E\,\Theta_A = 1.133\,\Theta_E\,\Theta_A$$

The error which is introduced by integrating eq. (I,2) from $-\infty$ to $+\infty$ rather than within the first minimum of the power pattern is less than 1%, if the gauss approximation holds down to a level of -20 dB. The main beam stray factor is defined by the integral

$$\text{(I,4)} \qquad \beta_m = \frac{1}{\Omega}\int_{\substack{\text{stray}\\ \text{region}}} f\, d\Omega = 1-\Omega_m/\Omega$$

The relation $\beta_m = 1-\Omega_m/\Omega$ follows immediately from eq. (I,1). The directivity of the antenna is $D = 4\pi/\Omega$, the gain is $G = \eta_R D = \eta_R 4\pi/\Omega$. The radiation efficiency η_R accounts for the ohmic losses in the feed and in the reflector. Inserting $\Omega = \Omega_m/(1-\beta_m)$ in the equation for the antenna gain, we obtain

$$\text{(I,5)} \qquad G = \eta_R(1-\beta_m)\frac{4\pi}{\Omega_m} = \eta_B\frac{4\pi}{\Omega_m}$$

The product

$$\text{(I,5)} \qquad \eta_B = \eta_R(1-\beta_m)$$

is defined as the beam efficiency and is one of the most important antenna characteristics for radio astronomical observations. The effective antenna area

$$A = \lambda^2/\Omega = \eta_B \lambda^2/\Omega_m \qquad (\lambda = \text{wavelength}) \tag{I,6}$$

can also be computed from beam efficiency and main beam solid angle. The aperture efficiency is the ratio of effective antenna area to geometrical aperture area and is hence $\eta_A = 4A/\pi D^2$ in the case of a circular aperture with diameter D. We obtain a very general relation between aperture efficiency and main beam efficiency

$$\eta_A = \eta_B \frac{4\lambda^2}{\pi\Omega_m D^2} \tag{I,7}$$

It follows from eq. (I,3) that $\Omega_m = \text{const} \cdot \lambda^2/D^2$, provided that the feed pattern does not depend on the wavelength. That means that aperture efficiency and beam efficiency differ by only a constant factor. For a feed taper of -16 to -18 dB, which is normally used in the NRAO telescopes, we have found the relation $\eta_A = 0.76\ \eta_B$ being valid, as long as the paraboloidal reflector can be considered perfect.

II. ANTENNA CONVOLUTION INTEGRAL

Any antenna can be considered as being located inside a black body enclosure whose wall temperature $T_b(\Theta,\varphi)$ is a function of the spherical

coordinates Θ,φ. The antenna temperature measured with the antenna pointing in the direction Θ,φ is given by the antenna convolution integral

$$T_A(\Theta,\varphi) = \frac{\eta_R}{\Omega} \left\{ T_b(\Theta,\varphi) * f(\Theta,\varphi) \right\} + (1-\eta_R) T_L \qquad \text{(II,1)}$$

The antenna characteristics η_R, Ω and f are defined in Appendix I. T_L is the physical temperature of the ohmic losses in feed and reflector.

The explicit form of the convolution integral becomes quite involved for spherical coordinates. If the convolution between radiation temperature $T_b(\Theta,\varphi)$ and antenna pattern in the stray region yields a only slowly varying contribution to the integral (II,1) so that it can be replaced by an approximately constant value $\eta_R \beta_m \overline{T_\beta}$ (with β_m the main beam stray factor and $\overline{T_\beta}$ an appropriate average value of the brightness temperature in the stray region), then the antenna pattern can be split up again in main beam and stray region (see Appendix I) in order to obtain a more convenient form of the antenna convolution integral.

We deal in the following with both point sources and extended sources, whose extension may be considerably larger than the main beam region of the antenna. We assume that the brightness temperature variation in the main beam region can be represented by the distribution $T_b(\xi,\eta) = T_b \psi(\xi,\eta)$. The distribution function is normalized so that $\psi_{max} = 1$ and T_b is consequently the maximum brightness temperature in the main beam region. The convolution integral can then be written in the form

$$(II,2)\qquad T_A(\xi,\eta) = \frac{\eta_B T_b}{\Omega_m} \int_{-\infty}^{+\infty}\int \exp\left\{ - \frac{(\xi-\xi)^2}{\xi_0^2} \frac{(\eta-\eta)^2}{\eta_0^2} \right\} \psi(\xi,\eta)\, d\xi\, d\eta$$

$$+ \eta_R \beta_m \bar{T}_\beta + (1-\eta_R) T_L$$

For the purpose of antenna measurements one is interested in: (i) the relation between effective antenna area A or beam efficiency η_B and the antenna temperature T_A produced by a radio source with known flux density S_ν or brightness temperature T_b, and (ii) the relation between the observed HPW of a drift curve Θ_A and the HPBW Θ_A of the antenna. Both relations can be obtained by evaluating the integral (II,2).

We consider the following brightness distribution functions which can be applied approximately to some of the calibration sources often used for antenna measurements [12].

Gaussian source distribution with HPW's Θ_s' and Θ_s''

$$(II,3a)\qquad \psi(\xi,\eta) = \exp\left\{ - \frac{\xi^2}{(0.6\,\Theta_s')^2} - \frac{\eta^2}{(0.6\,\Theta_s'')^2} \right\}$$

Disk distribution with radius R

$$(II,3b)\qquad \psi(\xi,\eta) = \begin{cases} 1 \text{ for } \sqrt{\xi^2+\eta^2} \leq R \\ 0 \text{ elsewhere} \end{cases}$$

Evaluating eq. (II,2) with these distributions yields for the HPBW Θ_A of the gaussian main beam in the direction of the drift

$$\Theta_A = \begin{cases} [\Theta_A'^2 - \Theta_s^2]^{1/2} & \text{for gaussian distribution with HPW } \Theta_s \\ [\Theta_A'^2 - \frac{\ln 2}{2}(2R)^2]^{1/2} & \text{for disk distrubution with diameter } 2R < \Theta_A \end{cases} \tag{II,4}$$

Θ_A' means the HPW of the observed drift curve.

In the mm-wavelength range it becomes difficult to find strong point sources for the measurement of the main beam pattern. It is possible, however, to determine the main beam pattern approximately from drift curves made with the sun or the moon [19]. If, especially, the antenna HPBW is less than about 3 minutes of arc and provided that the brightness temperature at the edge of the sun or the moon can be approximated by a step function, it can be shown that the differential quotient of the observed drift curve is proportional to the antenna pattern [22].

$$\frac{dT_A(\xi)}{d\xi} = \text{const.} \cdot f(\xi) \tag{II,5}$$

By computing the differential of the observed drift curve and normalizing its maximum value to unity, one obtains consequently the approximately true antenna pattern.

In order to find a relation between antenna temperature and brightness temperature or flux density, respectively, of a radio source, we define the source solid angle

$$\Omega_s = \int_{-\infty}^{+\infty}\int \psi(\xi,\eta)\,d\xi\,d\eta \tag{II,5a}$$

and the effective source solid angle

$$\Omega_s' = \int_{-\infty}^{+\infty}\int \psi(\xi,\eta)\, \exp\left\{-\frac{\xi^2}{\xi_o^2} - \frac{\eta^2}{\eta_o^2}\right\} d\xi d\eta \qquad \text{(II,5b)}$$

and obtain

$$T_A = \eta_B T_b \frac{\Omega_s'}{\Omega_m} = T_b \Omega_s' \frac{A}{\lambda^2} \qquad \text{(II,6a)}$$

$$S_\nu = \frac{2kT_A}{\lambda^2 \eta_B} \frac{\Omega_m \Omega_s}{\Omega_s'} = \frac{2kT_A}{A} \frac{\Omega_s}{\Omega_s'} \qquad \text{(II,6b)}$$

If the source HPW is small as compared to the antenna HPBW, $\Omega_s' \to \Omega_s$, and the source correction factor in eq. (II,6b) becomes unity.

The integrals (II,5a and b) have been evaluated for the distributions eq. (II,3a and b), assuming that the main beam has circular symmetry. If this is not the case the assumption $\Theta_A = \sqrt{\Theta_E \Theta_H}$ may still yield useful results in applying the following correction formulas

$$\Omega_s' = 1.133 \frac{\Theta_s' \Theta_s''}{[1 + \Theta_s'^2/\Theta_A^2]^{1/2} [1 + \Theta_s''^2/\Theta_A^2]^{1/2}} \qquad \text{(II,7a)}$$

$$\Omega_s/\Omega_s' = [1 + \Theta_s'^2/\Theta_A^2]^{-1/2} [1 + \Theta_s''^2/\Theta_A^2]^{-1/2}$$

for the gauss distribution, and

$$\Omega_s' = 1.133\ \Theta_A^2\ [1 - \exp\{-R^2/0.6\ \Theta_A)^2\}] \tag{II,7b}$$

$$\Omega_s/\Omega_s' = \frac{R^2}{(0.6\ \Theta_A)^2}\ [1 \exp\{-R^2/0.6\ \Theta_A)^2\}]$$

for the disk distribution.

III. BRIGHTNESS TEMPERATURES OF THE SURFACE OF THE EARTH AND THE ATMOSPHERE

In order to estimate the average temperatures in the different stray regions which enter in eq. (11), one has to know both the emissivity and temperature of the surface layer of the earth and of the atmosphere. It is clear that the emissivity of the surface of the earth depends on its roughness (as compared to a wavelength), on the angle of incidence and on the polarization angle. The main contribution to the radiation of the surface of the earth comes from the deeper layers beneath the surface, the longer the wavelength is, what has to be considered in an estimate of the physical temperature of the emitting regions. Some experimental work has been done in the field of direct measurements of the thermal radiation of the surface of the earth in the cm [23] and in the short dcm wavelength range [24][25]. Croom [26] gives a review of recent work in the field of antenna noise, and Hogg and Semplak [27] (Appendix B) have estimated the brightness temperature of the ground for three different models of the

surface emissivity. If the reflectivity of the ground is high a considerable part of the effective brightness temperatures of the sky is due to reflected sky radiation, an effect which has been used to reduce that part of the antenna temperature due to ground radiation [28].

The summary of both theoretical and experimental investigations shows that: (i) the emissivity of smooth surfaces (paved roads, buildings, metal plates, water, etc.) may deviate considerably from unity, (ii) the emissivity of surfaces may change very strongly with meteorological conditions (e.g., wet or snow-covered surfaces). But under the conditions of a dry surface whose roughness is random and large as compared to a wavelength and for angles of incidence which do not deviate too much from the normal to the surface, the emissivity of the surface of the earth is only a few percent less than unity, at least at shorter wavelengths. If these assumptions are not valid, however, a good estimate of the average brightness of the ground may be very difficult.

Both the thermal radiation of the atmosphere and the extraterrestrial radio radiation contribute to the brightness temperature of the sky. For frequencies higher than 1 GHz the contribution of the extraterrestrial radio radiation can be neglected (the brightness temperature of the coldest part of the sky is about 1.5°K at 1 GHz and decreases approximately with the frequency to the power -2.6) provided the main beam of the antenna is not too close to a strong radio source or to regions of enhanced brightness temperatures (Milky Way). The thermal radiation of the atmosphere depends on both the absorption and the average temperature of the air mass in the line of sight. Hogg [29] and Croom [26] have made

quite detailed computations of the brightness temperature of the atmosphere as a function of frequency and zenith distance. But for most practical purposes it can be assumed that the average air mass temperature $\overline{T}_{air}$ does not depend on the zenith distance, and that the brightness temperature of the atmosphere as a function of zenith distance z can therefore be presented in the form

$$T(z) = \overline{T}_{air}(1-p^{F(z)}) \qquad \text{(III,1)}$$

p is the transmission coefficient of the atmosphere at the zenith, F(z) is the air mass function which can be approximated for $z \leq 70°$ by $F(z) = 1/\cos z$. The transmission coefficient p depends on both the frequency and the amount of precipitable water in the atmosphere. Figure 8 shows values of -log p, computed by R. Menon [30] for the altitude of Green Bank, West Virginia, and for the best and worst observing conditions found at this place (excluded sky coverage by clouds). Extreme meteorological conditions excluded, $T_{air} \approx 260°K$ represents a fairly good value.

For $z \leq 30°$ is $F(z) \approx 1$ and hence the brightness temperature in this zenith region is practically identical with the temperature at zenith.

$$T_z = T(z = 0) = \overline{T}_{air}(1-p) \approx \overline{T}_{air} \frac{|\log p|}{0.4343} \qquad \text{(III,2)}$$

$$\text{for } |\log p| \ll 1$$

The average value of the thermal radiation of the atmosphere is obtained by computing the integral

$$(III,3) \qquad \bar{T}(z) = \bar{T}_{air} \frac{1}{2\pi} \int_{2\pi} (1-p^{F(z)})\, dS = \bar{T}_{air} \left[1 - \int_0^{\pi/2} p^{F(z)} \sin z\, dz\right]$$

This integral can be evaluated for $F(z) = 1/\cos z$, an approximation which yields, however, to small values of $p^{F(z)}$ for $z > 70°$. The average sky temperature computed in this way should be considered as an upper limit and numerical integration should be applied to obtain more accurate values. One obtains for $F(z) = 1/\cos z$.

$$(III,4a) \qquad \bar{T}(z) = \bar{T}_{air} \left[1-p + \ln p \cdot Ei\,(-|\ln p|)\right]$$

which has for $|\log p| \ll 1$ the convenient approximation

$$(III,4b) \qquad \bar{T}(z) = \bar{T}_{air}\, 2.3\, |\log p| \left\{1 + 2.3 \log \left[\frac{1}{4.1\, |\log p|}\right]\right\}$$

As may be seen from eq. (11), the average brightness temperatures of sky and ground enter into the expression of the total antenna temperature multiplied by the stray factor β_{II}. Assuming in this region a constant side lobe level (corresponding to the constant value f_{II} of the power pattern) one obtains from eq. (3a) $\beta_{II} = f_{II} \cdot \Omega\,(\text{Stray Region II})/\Omega$. Since $\Omega\,(\text{Stray Region II}) \approx 4\pi$ and $G = \eta_R 4\pi/\Omega$, we finally obtain

$$\beta_{II}\,\frac{\bar{T}(z)+\bar{T}_s}{2} \approx \frac{f_{II}\,G}{\eta_R}\cdot\frac{\bar{T}(z)+\bar{T}_s}{2} \qquad \text{(III,5)}$$

If the average side lobe level in the Stray Region II equals that of an isotropic radiator, then $f_{II}G = 1$; if the side lobe level is 10 dB below that of an isotropic radiator then $f_{II}\,G = 0.1$. With $|\log p| = 5.10^{-3}$ (corresponding to good observing conditions below 9 GHz) eq. (III,4) gives $\bar{T}(z) = 14.5°K$. Assuming $\bar{T}_g = 300°K$ and $\eta_R = 1$, the antenna temperature received in the Stray Region II is then $0.1 \cdot 157 = 15.7°K$. A similar estimate has been made by Hogg and Semplak [27].

REFERENCES

[1] Baars, J.W.M. and P.G. Mezger, NRAO El.Div.Int.Rep.No.30, May 1964

[2] Ruze, J., "Physical Limitations on Antennas," Tech.Rep. 248, Res. Lab. of Electronics, MIT, October 1952

[3] Skolnik, M.I., "Introduction to Radar Systems," McGraw-Hill, 1962, Chapter 7

[4] Jasik, H. (Editor) "Antenna Engineering Handbook," McGraw-Hill, 1961, Chapter 2

[5] Scheffler, H., Z.f.Astrophys. 55, 1, 1962

[6] Seeger, Ch.L., G. Westerhout and H.C. van de Hulst, BAN 13, 172, 1956

[7] Mezger, P.G., Telefunken Ztg. 124, 99, 1959

[8] Kuzmin, A.D. and A.E. Salomonovich, "Radio Astronomical Method of the Measurement of Antenna Parameters" (in Russian),1964

[9] Bracewell, R.N., "Radio Astronomy Techniques," in "Handbuch der Physik" Vol. LIV (S. Fluegge, editor), Springer, 1962

[10] Ko, H.C., IEEE Trans. Ant. & Prop. AP-12, 902, 1964

[11] Howard, W.E.,III, T.R. Dennis, S.P. Maran, and H.D. Aller, Ap.J. Suppl.

[12] Baars, J.W.M., P.G. Mezger and H.Wendker, Ap.J. in press

[13] Mayer, C.H., IEEE Trans. Ant.& Prop. AP-12, 902, 1964

[14] Findlay, J.W.,"Advances in Radio Research,", Vol. 2, pp. 37-119, Academic Pre

[15] Schoenberg, E., Handbuch der Astrophysik Bd.II, p. 268, 1929

[16] Kelleher, K.S. and H.P. Coleman, NRL Report 4088, Dec. 1952

[17] Ruze, J., "Lateral Feed Displacement in a Paraboloid," paper presented at Session V-4 PTGAP Int. Symposium, New York,1964

[18] Ross, D. and Y. Terzian, NRAO El.Div.Int.Rep.No. 37, Oct. 1964

[19] Stumpff, P., In preparation

[20] Bracewell, R. N., IRE Trans. Ant. and Prop. AP-9, 49, 1961

[21] Ruze, J., "Reflector Tolerance Determination by Gain Measurement," NEREM, Nov. 6, 1964, Session M-5.4

[22] Baars, J.W.M. and P.G. Mezger, NRAO El.Div.Int.Rep.No. 36, Oct. 1964

[23] Hachenberg, O., Das Bild des Erdbodens in seiner thermischen Eigenstrahlung im cm-Wellengebiet. Akademieverlag Berlin, 1958

[24] Mezger, P.G., Z.f.angew, Physik 11, 41, 1959

[25] Mezger, P.G., Mitteilung der Sternwarte Bonn Nr.59, T.III

[26] Croom, D.L., Proc. IEEE 3, 967, 1964

[27] Hogg, D. C. and R.A. Semplak, BST 43, 2677, 1964

[28] Pauliny-Toth, I.I.K., I.R. Shakeshaft and R. Wielebinski, Proc. IRE 50, 2483, 1962 (cor.sp.)

[29] Hogg, D.C., Jour. of Apl. Phys. 30, 1417, 1959

[30] Menon, R., Atmospheric Absorption in the Range of Wavelength Between 10 cm and 1 Micron, NRAO Int. Rep., January 1964

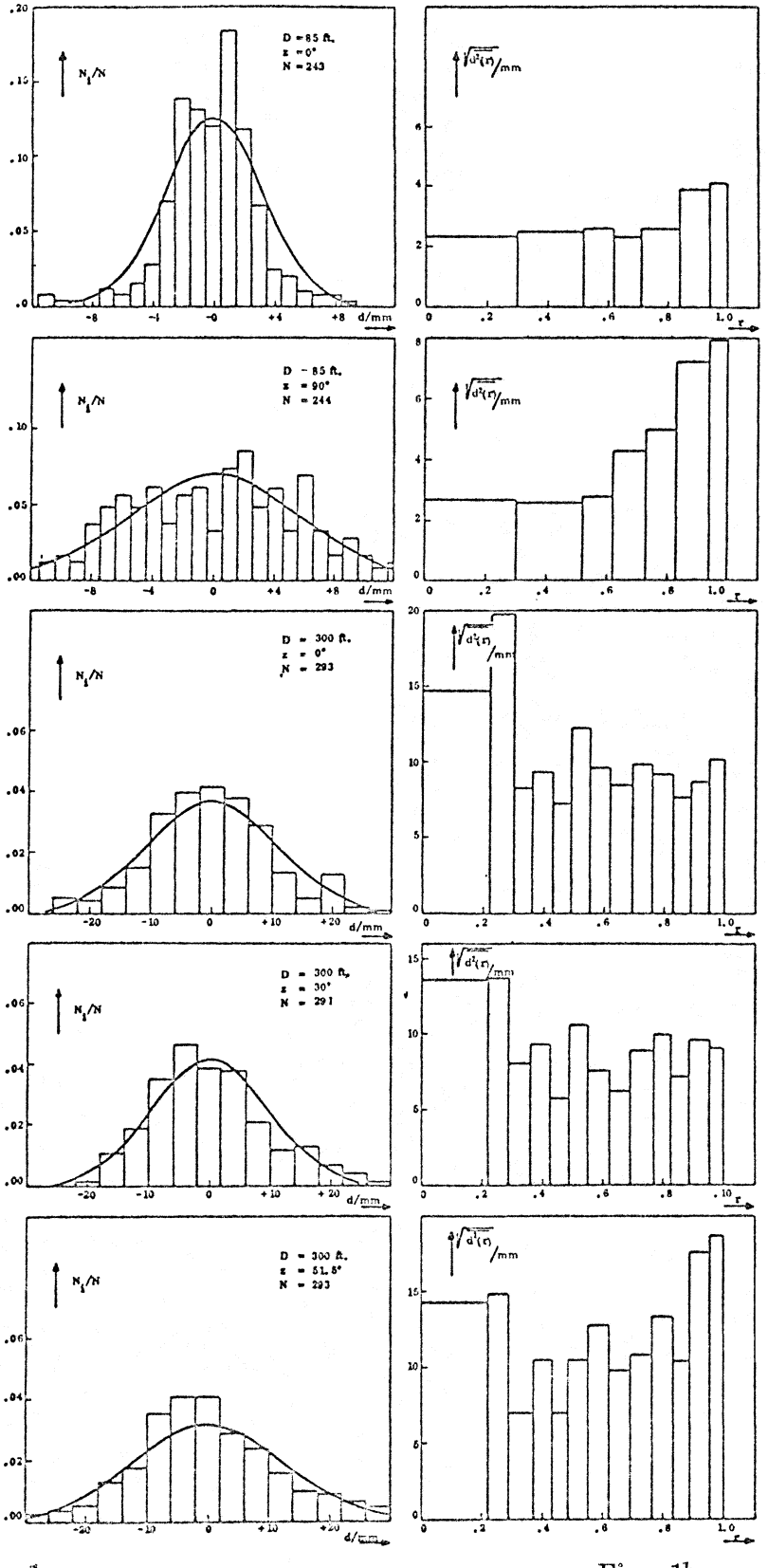

Fig. 1a

Histogram of the relative number of deflections of the 85(I)-foot and of the 300-foot reflector within various deflection intervals.

Fig. 1b

Histogram of the R.M.S. deviations of various ring-shaped zones of the 85(I)-foot and of the 300-foot reflector plotted as a function of the normalized distance in the aperture plane.

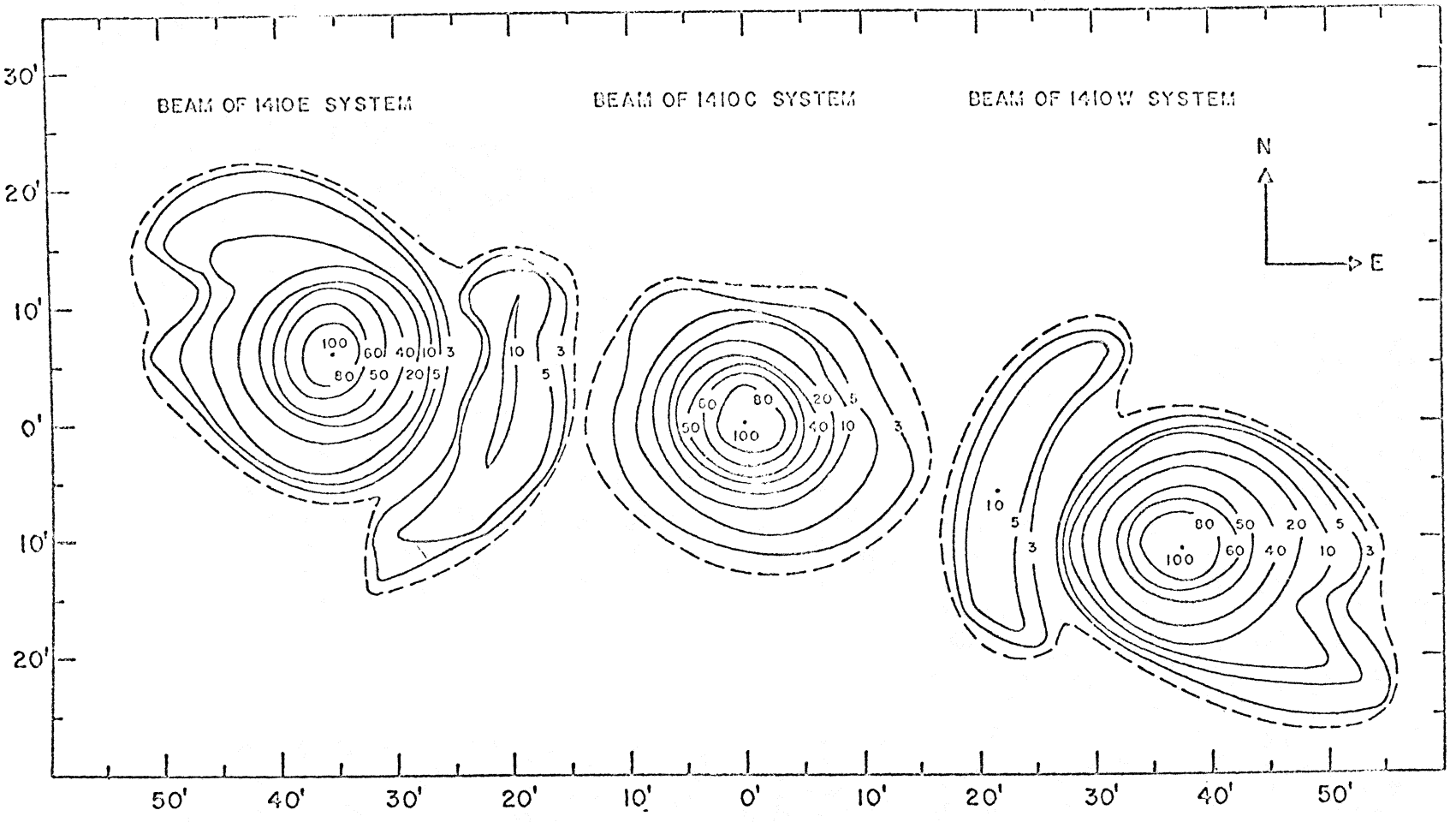

Fig. 2. Main beam and coma lobe of three identical horn feeds in the focal plane of the 300-foot telescope. The East and West feeds are displaced corresponding to a beam tilt of 3.55 and 3.9 times the HPBW of the central feed. [18]

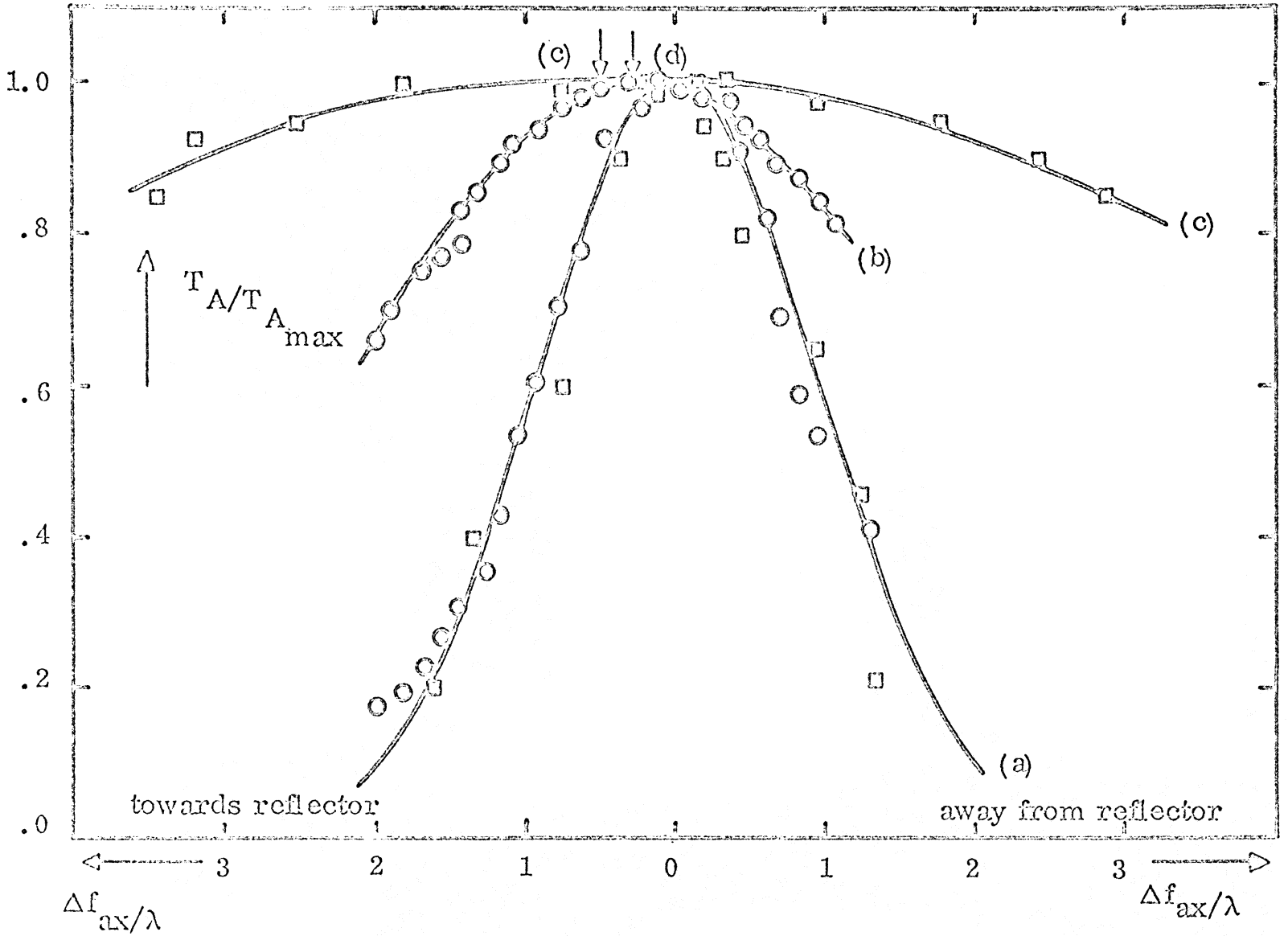

Figure 3 : Relative change of antenna temperature measured with the 85(I)-foot telescope at 6 GHz (oo) and at 14.5 GHz (□□). Curve a: measured with a point source; Curve b and c: measured with the moon.

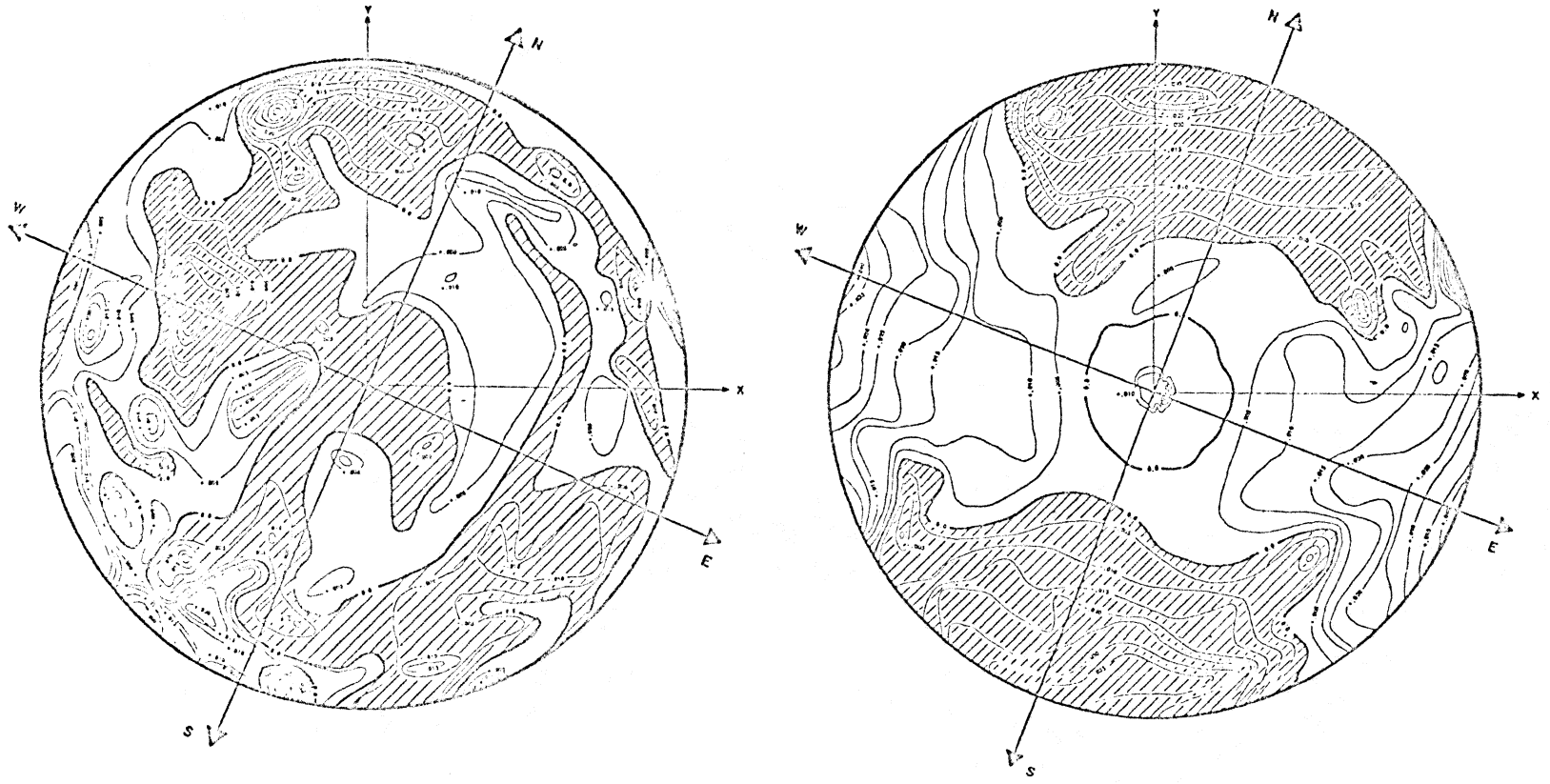

Z = 0°

Z = 90°

Figure 4: Contour map representation of the measured deviations of the 85(I)-foot reflector at the zenith distances z = 0° and z = 90°. The cross-hatched areas correspond to deviations in the direction opposite to the focal point. 1 contour interval = 0.005 ft = 1.5 mm.

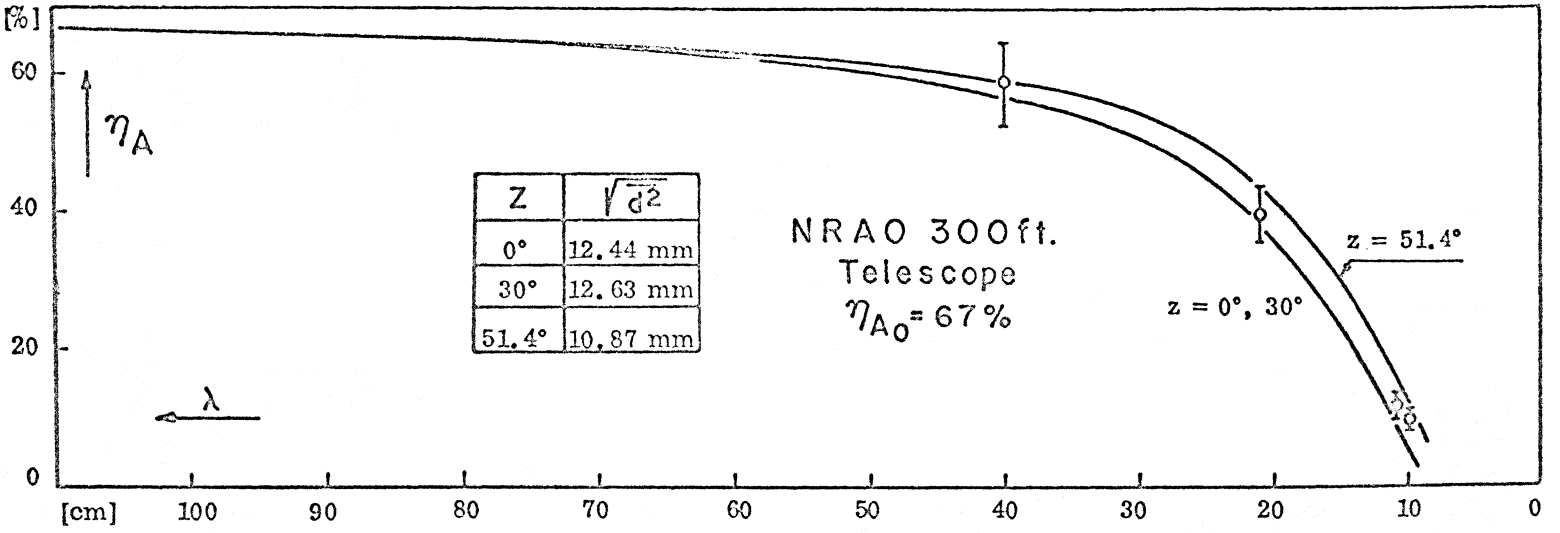

Fig. 5a: Computed and measured aperture efficiency of the 300-foot telescope

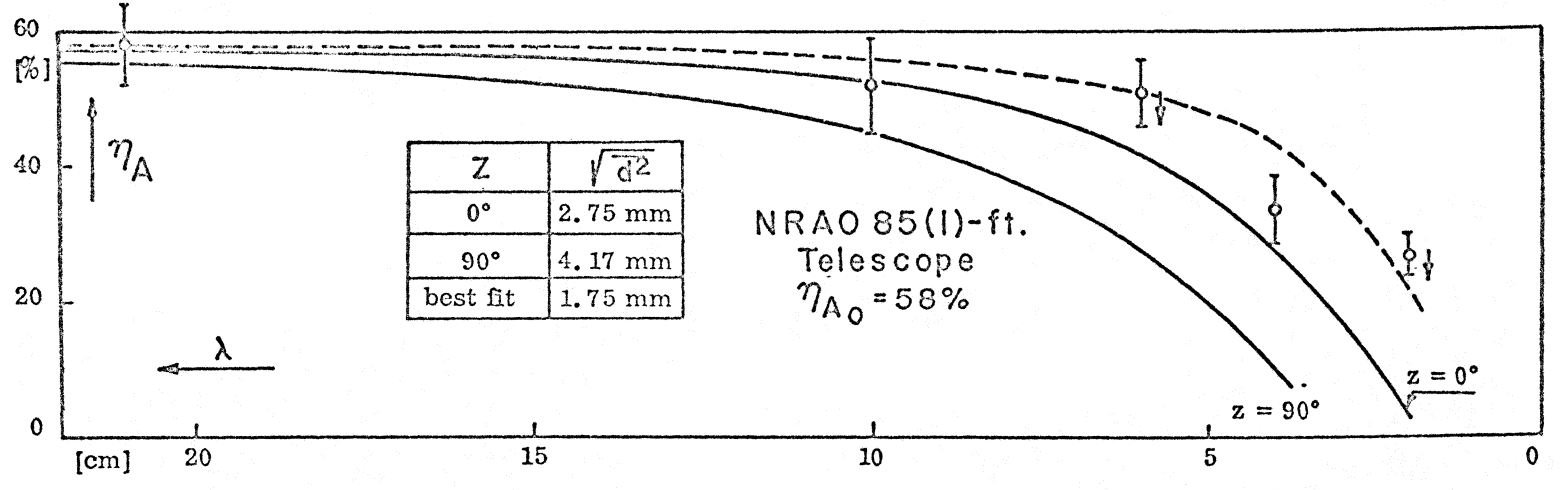

Fig. 5b: Computed and measured aperture efficiency of the 85(I)-foot telescope

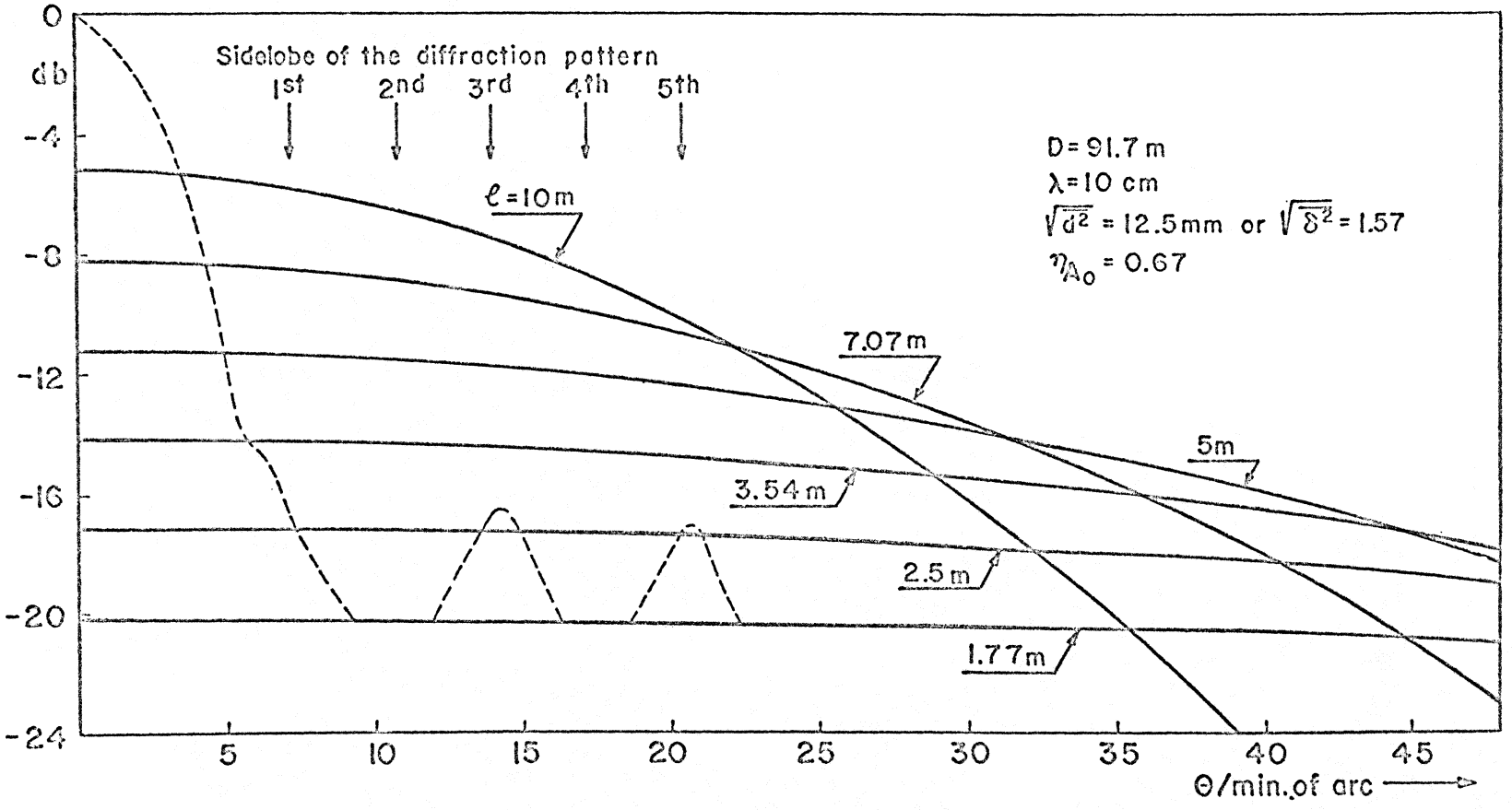

Fig. 6 Error pattern of the 300-foot telescope computed for various correlation lengths (full curves) and cross section through the main beam and the first side lobes measured with a point source. (dashed curve)

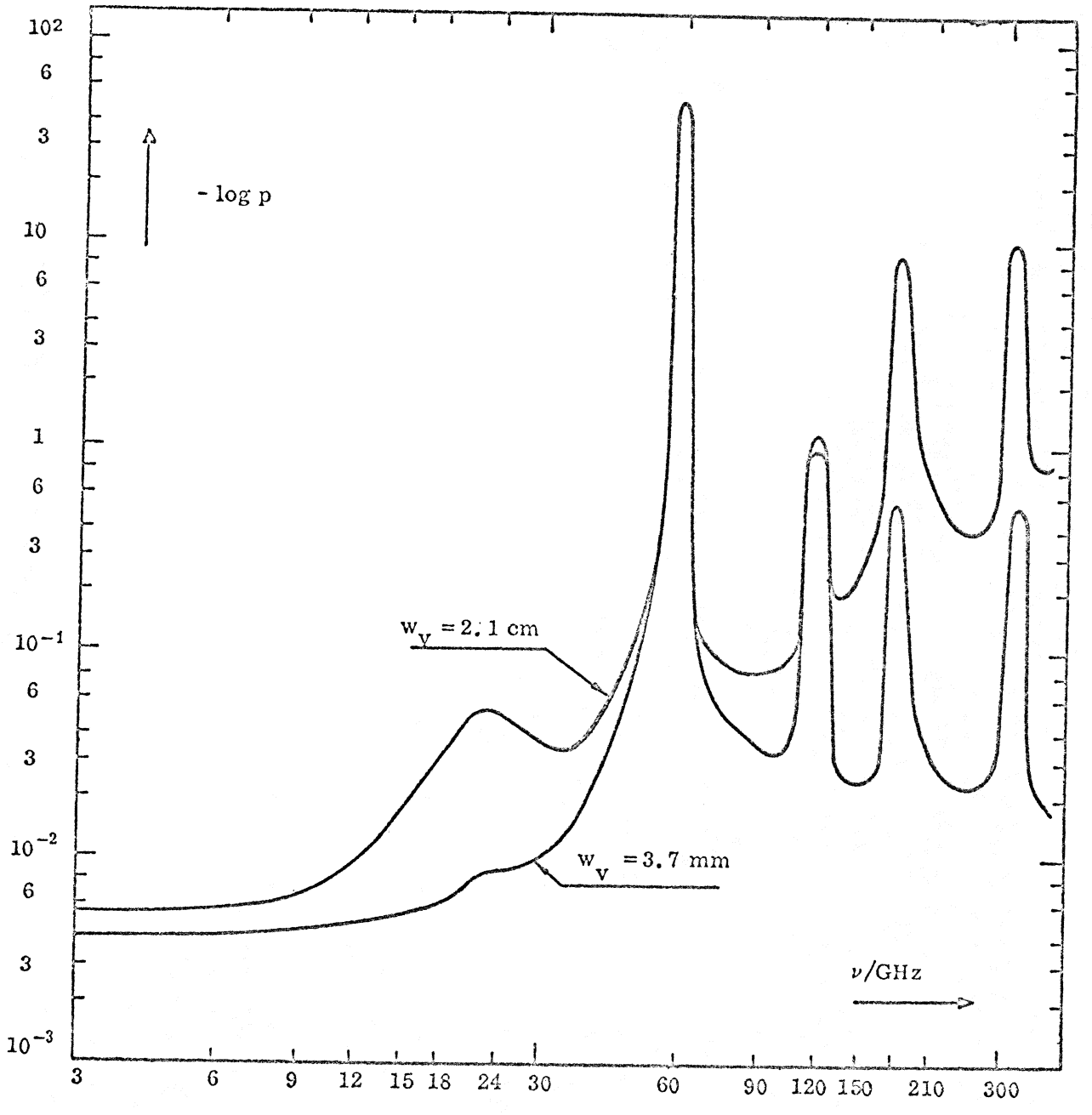

Fig. 7 Logarithm of the zenith transmission coefficient of the atmosphere as a function of frequency. Computed by R. Menon [30] for the altitude of Green Bank, W. Va. (833 m) and for two different amounts of precipitable water in the atmosphere.